Lab on a Chip

Cite this: *Lab Chip*, 2012, **12**, 2874–2880

www.rsc.org/loc

PAPER

SSA-MOA: a novel CTC isolation platform using selective size amplification (SSA) and a multi-obstacle architecture (MOA) filter†

Minseok S. Kim,[a] Tae Seok Sim,[a] Yeon Jeong Kim,[a] Sun Soo Kim,[b] Hyoyoung Jeong,[a] Jong-Myeon Park,[ac] Hui-Sung Moon,[a] Seung Il Kim,[d] Ogan Gurel,[e] Soo Suk Lee,*[a] Jeong-Gun Lee*[a] and Jae Chan Park[a]

Received 16th January 2012, Accepted 8th May 2012
DOI: 10.1039/c2lc40065k

Circulating tumor cells (CTCs) have gained increasing attention as physicians and scientists learn more about the role these extraordinarily rare cells play in metastatic cancer. In developing CTC technology, the critical criteria are high recovery rates and high purity. Current isolation methods suffer from an inherent trade-off between these two goals. Moreover, ensuring minimal cell stress and robust reproducibility is also important for the clinical application of CTCs. In this paper, we introduce a novel CTC isolation technology using selective size amplification (SSA) for target cells and a multi-obstacle architecture (MOA) filter to overcome this trade-off, improving both recovery rate and purity. We also demonstrate SSA-MOA's advantages in minimizing cell deformation during filter transit, resulting in more stable and robust CTC isolation. In this technique, polymer microbeads conjugated with anti-epithelial cell adhesion molecules (anti-EpCAM) were used to selectively size-amplify MCF-7 breast cancer cells, definitively differentiating from the white blood cells (WBCs) by avoiding the size overlap that compromises other size selection methods. 3 μm was determined to be the optimal microbead diameter, not only for size discrimination but also in maximizing CTC surface coverage. A multi-obstacle architecture filter was fabricated using silicon-on-glass (SOG) technology—a first such application of this fabrication technique—to create a precise microfilter structure with a high aspect ratio. The filter was designed to minimize cell deformation as simulation results predicted that cells captured *via* this MOA filter would experience 22% less moving force than with a single-obstacle architecture. This was verified by experiments, as we observed reliable cell capture and reduced cell deformation, with a 92% average recovery rate and 351 peripheral blood leukocytes (PBL) per millilitre (average). We expect the SSA-MOA platform to optimize CTC recovery rates, purity, and stability, increasing the sensitivity and reliability of such tests, thereby potentially expanding the utilization of CTC technologies in the clinic.

1. Introduction

Metastasis, the spread of cancer from a primary tumor to a distant site, is largely responsible for cancer's lethality. Research into circulating tumor cells (CTCs) has suggested an important role for these cells in metastatic spread, inspiring hope of new and more effective ways to diagnose and treat aggressive disease.[1] Detection of these exceedingly rare cells within the circulation may provide important clues regarding cancer prognosis and progression, potentially advancing, too, the assessment of anticancer drug treatment and optimization of individualized therapy.[2] Although the application of CTC technology holds much promise, significant discrepancies among capture methods may lead to wrong expectations as clinical studies—in advanced breast cancer, for example—have indicated a 5 cells ml^{-1} cut-off level between a favorable or poor prognosis.[3] More robust systems are required for the reliable isolation of these very scarce cells and to realize the clinical potential of CTC assays.

The principal technical challenge in CTC enumeration and analysis arises from the extraordinary rarity of these CTCs in the bloodstream, complicated by the millions of WBCs, billions of erythrocytes, and the myriad of other molecules—known and unknown—also present in blood.[4] Presently a wide variety of

[a]*POCT In Vitro Diagnostics Group, Bio Research Center, Samsung Advanced Institute of Technology (SAIT), Samsung Electronics Co., Ltd., San 14, Nongseo-dong, Giheung-gu, Yongin-si, Gyeonggi-do, Republic of Korea. E-mail: soosuk@samsung.com; biogun.lee@samsung.com*
[b]*R&D Solution group, Samsung Advanced Institute of Technology (SAIT), Samsung Electronics Co., Ltd., San 14, Nongseo-dong, Giheung-gu, Yongin-si, Gyeonggi-do, Republic of Korea*
[c]*Department of Chemistry and Center for Bioactive Molecular Hybrids, Yonsei University, Seoul, 120-749, Republic of Korea*
[d]*Department of Surgery, Yonsei University College of Medicine, 134 Shinchon-dong, Seodaemun-gu, Seoul, Republic of Korea*
[e]*CTO Office – MOT Research Center, Samsung Advanced Institute of Technology (SAIT), Samsung Electronics Co., Ltd., San 14, Nongseo-dong, Giheung-gu, Yongin-si, Gyeonggi-do, Republic of Korea*
† Electronic supplementary information (ESI) available. See DOI: 10.1039/c2lc40065k

CTC isolation concepts and systems exist including nucleic acid-based detection,[5] direct interaction *via* antibodies and microposts,[6,7] immunomagnetic separation,[4,8,9] density gradient,[10,11] size filtration,[12–16] dielectrophoresis (DEP)[17] and flow cytometry.[18] In density gradient methods, a medium such as Ficoll separates CTCs from other blood cells on the basis of their differential densities. Immunomagnetic techniques, including the CellSearch™ system, bind nanomagnetic particles to EpCAM+ cells, sequestering these CTCs *via* magnetic forces. Both methods, however, require a removal step for any residual blood cells, which entails cell loss and poses reproducibility challenges. In yet another approach, the micropost technique, which has demonstrated high purity rates, CTCs are directly bound to micropost-adherent antibodies. This platform depends, however, on the probability of interaction between the transiting cells and the intervening microposts, a statistical contingency that makes the collection of very rare CTCs quite difficult.

Size-based separation of CTCs, based on the fact that epithelial-derived tumor cells are generally larger than peripheral blood leukocytes, has also seen recent—and promising—application.[12] Compared to other methods, size-based platforms, including membrane-based and microfluidic filters systems, have shown superior recovery rates. Yet, size filtration suffers from a fundamental trade-off between recovery rate and purity, with purity being limited as significant quantities of WBCs remain sequestered within the filter.[2] Moreover, given the heterogeneity of CTCs—varying in cell dimensions as well as their molecular characteristics[19]—smaller sized CTCs would pass unhindered through the filters. Therefore, developing a stable and reliable CTC isolation method that guarantees both high recovery rates *and* high purity is of critical importance in developing clinical applications, including assessing cancer progression and prognosis as well as personalizing treatment.[20]

Here we introduce a new CTC capture concept based on combining a size-based separation method with a novel multi-obstacle filter architecture achieving reliable CTC isolation with high recovery rates and high purity. The method comprises two processes in sequence: first, selective size amplification (SSA) of the circulating cancer cells *via* CTC-specific microbeads to more clearly discriminate (*e.g.* without size overlap) between CTCs and the much more numerous white blood cells and, second, passing this microbead treated sample through a multi-obstacle architecture (MOA) microfluidic filter. By selectively amplifying the CTC size with solid microbeads *before* microfiltration, the trade-off between recovery rate and purity attributable to size-based isolation can be overcome. To also address problems with previous filter architectures, a novel multi-obstacle platform was designed for stable cell capture and to reduce the mechanical stress exerted upon cells passing through the filter. We implemented a silicon-on-glass (SOG) technology—which we believe, in this case, to be a first such application—to create an accurate filter gap even given the high-aspect ratio structure and to enable, too, clearer cell visualization under optical microscopy. Using these advances, solid melamine microbeads conjugated with anti-EpCAM were specifically adhered to EpCAM+ cancer cells and it was confirmed that the size-amplified cancer cells resulted in higher recovery rates and more stable capture as compared to conventional microfiltration methods.

2. Materials and methods

2.1 Ethics statement

Human blood samples were obtained from Yonsei University (Seoul, Korea). In all cases, informed written consent was obtained from all participants and this study was approved by the Institutional Review Board (IRB) at the Yonsei University, Seoul, Korea. We are especially grateful to all clinical study participants and hope that their contributions will help advance, *via* improved CTC capture techniques, cancer diagnosis and treatment.

2.2 Cancer cells and microbead preparations

Two commercially available breast carcinoma cell lines, MCF-7 and MDA-MB-231, were obtained from American Type Culture Collection (ATCC; Manassas, VA). MCF-7 and MDA-MB-231 were maintained in Dulbecco's Modified Eagle Medium (DMEM) and RPMI-1640 supplemented with 10% fetal bovine serum (FBS), 100 IU ml^{-1} penicillin, and 100 mg ml^{-1} streptomycin, respectively. All cell lines were cultivated at 37 °C and incubated in 5% CO_2 conditions. Adherent cells were harvested by trypsinization before reaching confluence. To acquire human primary leukocytes, the density gradient reagent (Ficoll-Paque plus, GE Healthcare Inc.) was carefully layered upon the whole blood and the upper layer of the Ficoll reagent was obtained after centrifugation at 1000*g* for 30 min.

Solid melamine microbeads were obtained from Postnova Analytics Inc. The microbeads were reacted with a carbodiimide (EDC)/*N*-hydroxysuccinimide (NHS) coupling kit (Biacore, BR-1000-50, MA) in an Eppendorf tube. After washing with 2-(*N*-morpholino)ethanesulfonic acid (MES) buffer, protein G in phosphate buffer saline (PBS) was added to improve orientation of anti-EpCAM and the tube was rotated for two hours. After washing with PBS, the microbeads were treated with anti-EpCAM (R&D Systems, MA) for another two hours. Conjugating the microbeads with anti-EpCAM improved the efficiency of microbead adherence with the CTCs.

2.3 Fabrication of the MOA filter

The MOA filter was fabricated by silicon-on-glass (SOG) technology in order to create a precise filter gap. Briefly, silicon and glass wafers were bonded using anodic methods; lapping and chemical mechanical polishing (CMP) were performed on the silicon layer. This process determined the filter height with the 50 μm thickness of the Si layer remaining constant throughout this study. Photoresist, AZ 4330 (Clariant Corp., NJ), was patterned and deep reactive-ion etching (DRIE) was performed for 15 min. After H_2SO_4 cleaning, a glass wafer was laminated and patterned using a dry film photoresist, Ordyl BF 410. When the sandblasting process was completed for the inlet and outlet ports, the capping glass wafer was aligned and connected with the Si-glass wafer by anodic bonding.

2.4 Identification of CTCs and image analysis

An Olympus IX81-ZDC inverted microscope with a motorized stage was used to image the active area in a microfluidic MOA filter chip. After completing the blood filtration step, fixation

and permeabilization processes were conducted with 4% paraformaldehyde for 20 min and 0.01% Triton X-100 solutions for 10 min, respectively. Staining reagents including DAPI, anti-cytokeratin PE (CAM 5.2, BD Biosciences, CA) and CD45 FITC (BD Biosciences, CA) were treated for 60 min and then washed with PBS. The microfilter was scanned automatically for the active area of an MOA filter chip. Captured images were carefully examined and the cells that stained positive for cytokeratin and negative for CD45 were scored as CTCs with consideration of the phenotypic morphological characteristics.

Laser total internal reflection fluorescence (TIRF) microscopy (Carl Zeiss, Germany) was used to investigate cell–bead binding using the bright field z-stack function. Using the multidimensional acquisition mode of AxioVision (AxioVs40; Carl Zeiss, Germany) software, at least 50 z-stack images for a CTC covered with microbeads were acquired where the center of a CTC was initially focused and the z-stack height set to $\pm$ 25 μm (slice distance: less than 1 μm). Bead coverage was calculated using image analysis software (ImageJ program, NIH). Twenty five images of cells covered with microbeads were acquired, and for each image the total cell surface area and the surface area occupied with microbeads was calculated. Bead coverage was defined as the percent ratio of the area occupied with microbeads (conjugation area) divided by the total area of the cell and microbeads (total area, Supplementary Fig. 1, ESI†). A high speed camera (Fastcam SA5, Photron Inc., CA) was used to dynamically image the cells as they passed through the MOA filter. Images were acquired at a resolution of 512 $\times$ 512 pixels and a frame rate of 500 s^{-1}.

3. Results and discussions

3.1 Selective size amplification of CTCs

Size-based separation, based on the premise that CTCs are *often larger* than native leukocytes, has been a leading technique for CTC isolation.[12] The simplicity of the technique also offers compelling advantages. The operative term 'often larger', however, handicaps this approach with low purity because of the variability of tumor cell size and, moreover, the overlap of these sizes with white blood cells.[19] We therefore introduce a novel approach that *amplifies* the CTC size in order to definitively differentiate them from WBCs, subsequently isolating these size-amplified CTCs *via* an efficient microfilter (Fig. 1). By selectively size-amplifying CTCs, these cells are transformed from being 'often larger' to *always larger*, thus allowing size-based separation to achieve higher recovery rates and purity.

We characterized the size amplification of breast cancer cells (MCF-7) as a function of microbead size. Fig. 2A shows the size distributions of WBCs, MCF-7 and the MCF-7 covered with microbeads of varying size. Although the average WBC diameter was 8.5 μm, there was considerable size variability with some leukocytes, monocytes and granulocytes in particular, reaching diameters up to 17 μm. Native MCF-7 breast cancer cells were observed to have average diameters of 16.6 $\pm$ 2.3 μm (n = 25), partially overlapping in size, therefore, with WBCs. In contrast, MCF-7 cells size-amplified with anti-EpCAM conjugated microbeads could be positively discriminated from WBCs. Size amplification increased monotonically as a function of microbead diameter as the MCF-7 cells conjugated with 1, 2, 3, 4, and 5 μm microbeads were 20.1, 22.1, 25.4, 25.9, and 26.5 μm in average diameter, respectively.

We also evaluated the surface coverage of microbeads. Coverage was quantified by image analysis as a percentage ratio of microbead area to total single cell area. Fig. 2B exhibits CTCs covered with microbeads of varying diameters. While melamine microbeads showed nice coverage over 80% and stable binding with cancer cells until 3 μm melamine microbeads, the coverage was significantly decreased from the 4 μm microbeads and unstable binding was exhibited, increasing variation of coverage. The unstable binding and increased coverage variability (as observed in bead binding images) for the 4 μm and 5 μm microbeads may result from a sphere packing issue. Moreover, the decreased ratio of microbead–CTC contact area relative to microbead mass might also appear to be a major cause for this phenomenon. From the result, the optimal bead size for selective size amplification was decided to be the 3 mm melamine bead by considering both size amplification and bead coverage.

To verify our approach in a realistic context, we applied selective size amplification with microbeads to human primary leukocytes, EpCAM-negative cell line (MDA-MB-231), and EpCAM-positive cell line (MCF-7). The anti-EpCAM microbeads bound only to MCF-7 cells (Supplementary Fig. 2A, ESI†) while the breast cancer cells and white blood cells displaying negative EpCAM expression did not interact with the microbeads (Supplementary Fig. 2B and 2C, ESI†). Therefore, we confirmed that the modified microbeads were specifically bound with EpCAM expressed cells.

3.2 Design of the MOA filter and system automation

CTCs are rare and several studies have reported that these epithelium-originated cells are unstable, with only a short half-life within the circulation.[21,22] Therefore, cytocompatible isolation with minimal stress is urgently needed to satisfy accurate clinical investigation of CTCs. The novel multi-obstacle architecture (MOA) filter was designed for stable cell collection with minimal mechanical stress, improving the recovery rate. Several microfluidic cell isolation techniques have been developed using microstructures such as cell docking, point pillars, rectangular or single obstacle architectures.[14,15,23] With these techniques, the captured cells could occasionally become jammed between filter structures and escape due to subtle pump fluctuations or unexpected external collisions. In the case of the MOA filter, however, a ''cell capture room'' situated between the first and second filter gaps mitigated jamming and ensured stable capture even with unwanted vibrations.

Computational fluid dynamics (CFD) simulation was conducted for the pressure distribution of captured cells as a function of different filter shapes and captured positions. Compared to cells sequestered by a single-obstacle filter (Supplementary Fig. 3A, ESI†), those captured by MOA filters were calculated to experience 22% less moving force. In addition, when a cell was positioned at the second obstacle of the MOA filter (Supplementary Fig. 3C, ESI†), the mechanical stresses exerted upon the cell was reduced by 23% (Table 1), confirming the MOA filter's ability to reduce hydrodynamic stresses upon captured cells, facilitating, therefore, stable isolation.

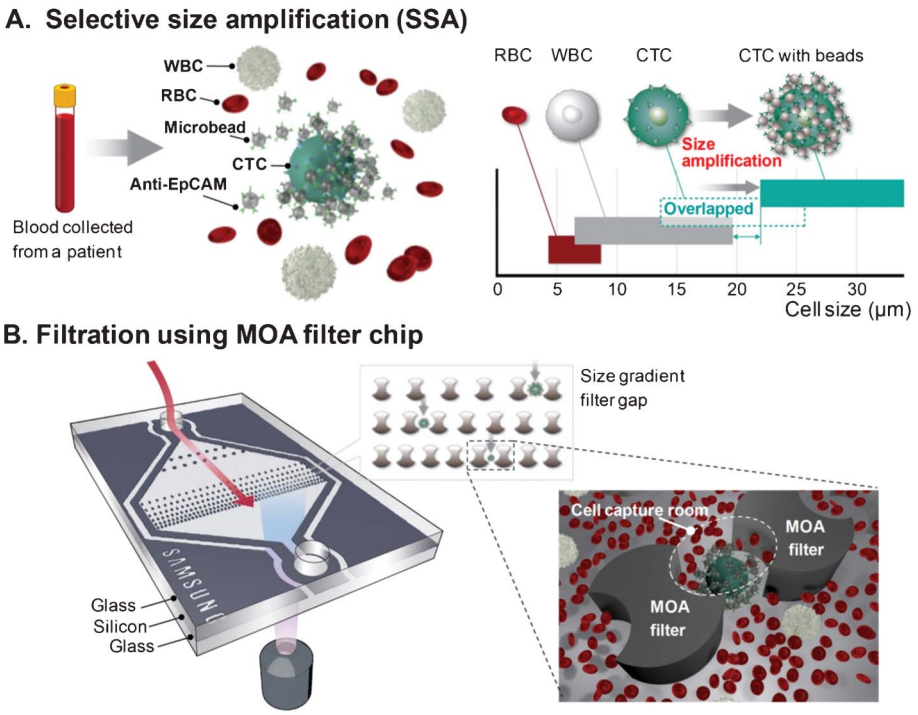

Fig. 1 Schematic of a novel CTC separation technique using selective size amplification (SSA) and multi-obstacle architecture (MOA) microfiltration. (**A**) Selective size amplification using solid microbeads conjugated with anti-EpCAM. While CTCs ordinarily overlap in size with WBCs, this distribution can be differentiated by amplifying the CTC dimensions *via* the binding of CTC-specific microbeads. (**B**) Multi-obstacle architecture (MOA) size-gradient filter chip. The MOA filter unit has two filter gaps and jamming of cells is mitigated by a "cell capture room" between the first and second filter gaps. The MOA chip was fabricated by silicon-on-glass (SOG) technology.

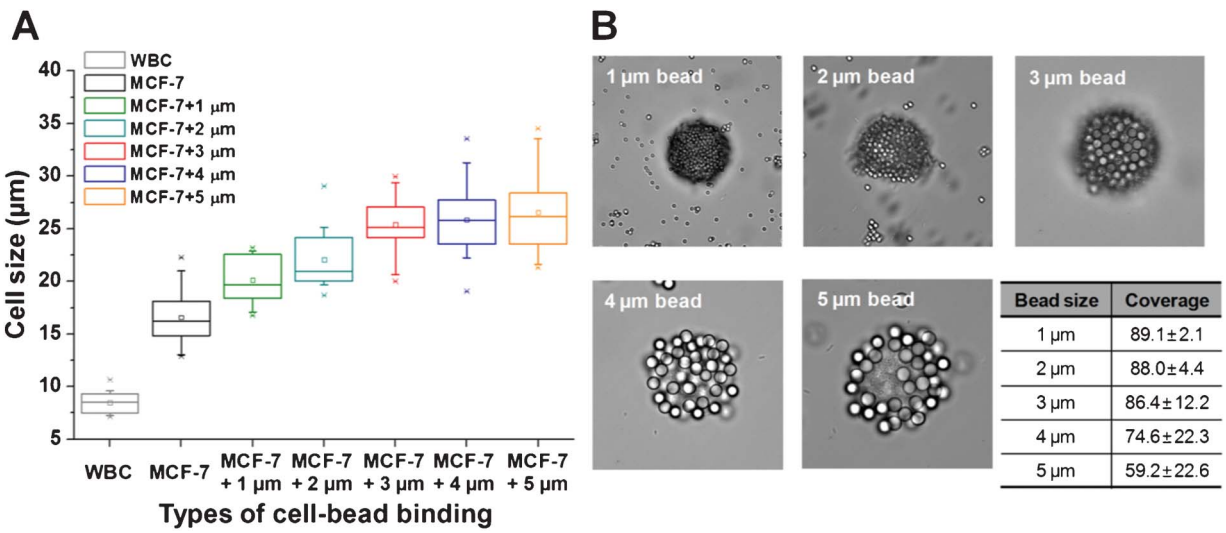

Bead size	Coverage
1 μm	89.1±2.1
2 μm	88.0±4.4
3 μm	86.4±12.2
4 μm	74.6±22.3
5 μm	59.2±22.6

Fig. 2 Characterization of size amplification for breast cancer cells as a function of microbead size. (**A**) Box chart for size distributions of WBCs, MCF-7 and the MCF-7 covered with 1, 2, 3, 4, and 5 μm melamine microbeads, respectively (n = 25). From the 3 μm microbead, the cell size was apparently increased compared to native cancer cells. (**B**) MCF-7 cells covered with 1, 2, 3, 4, or 5 μm melamine microbeads. Images (25 images for each) were obtained with laser total internal reflection fluorescence (TIRF) microscopy at 1000× magnification with microbead treatment. Melamine microbeads ranging in size from 1 to 3 μm showed good coverage (>80%) and stable cancer cell binding, though at 4 μm and larger, coverage significantly declined and unstable binding was also observed (n = 25).

The MOA unit filters were arranged in a zigzag fashion to maximize cell manoeuvrability (pathway freedom) which reduces cell stacking, thereby improving purity. In addition, we constructed different filter gaps in order to further minimize cell stress among cells of different sizes. In this case, given the anticipated dimensions of size-amplified CTCs, we constructed the MOA filter gap to range between 8 μm to 30 μm. Because many reports have shown that CTC numbers in the tens or

Table 1 Comparisons of forces and stresses applied to captured cells as a function of filter shapes and captured positions. Forces and stresses are pN and N m^{-2} units, respectively

Types	Pressure force	Shear force	Pressure stress	Shear stress	Force sum	Stress sum
Single-obstacle filter	3.11	1.34	8.79	0.74	445	9.53
Multi-obstacle filter 1st	2.46	9.40	10.41	0.52	340	10.93
Multi-obstacle filter 2nd	2.4	1.11	6.69	0.64	350	7.33

hundreds are sufficient to predict a poor prognosis,[24–27] we designed the MOA chip with 3900 filters giving an active capture area of 10.8 mm × 3.6 mm, 25 times smaller in area than the CTC chip.[6] In particular, miniaturizing the active area reduced the analysis time which included multi-color image acquisition and cell counting.

Since CTC analysis is performed on whole blood samples, it is important to remove areas of stagnation in a microfluidic filter, especially for the purposes of maximizing purity. The issue could be solved by designing a curved shape for the forward and backward areas of the filter. When the microfluidic filter height increases, throughput can be increased. The resulting irregular focusing position, however, made the cell count and biochemical analyses more difficult. Therefore, we analyzed the pressure force applied to the filter and cells as a function of filter heights. CFD simulations showed that the pressure forces exerted upon cells drop significantly at filter heights between 30 μm and 50 μm (Supplementary Fig. 4, ESI†). Filter heights beyond 50 μm negligibly impacted pressure forces, so, in consideration of cell stress and based on microscopic analysis, we determined the optimal filter height to be 50 μm.

As a precisely machined filter gap is the most critical factor for microfluidic filters, we sought to manufacture a very accurate microfilter structure with a high-aspect ratio. Elastomer casting such as polydimethylsiloxane (PDMS) poses several problems including difficulties in full development of the photoresist owing to a number of factors (high-aspect ratio and elastomer detachment from the mold, unknown dust in microfilters, and unstable tube connection) all of which challenge scale-up and mass production. Therefore we used, in what we believe to be the first such application, silicon-on-glass (SOG) technology to fabricate the CTC microfilter chip (Supplementary Fig. 5A, ESI†). This method offered a number of advantages as compared to conventional silicon fabrication: an unobstructed optical microscopic view of the cells in transit, precise microfilter fabrication, dust minimization, robust interconnection *via* a solid-state filter chip, and anticipated ease of commercialization. The fabricated device was directly connected with an inlet and outlet using a manifold, being fed in turn by an automatic fluid control system (Supplementary Fig. 5B, ESI†). For CTC isolation and biochemical assays, several steps were sequentially implemented for chip priming for bubble removal, BSA coating, whole blood processing, washing to remove residual blood cells, fixation, permeabilization, cell staining, and washing.

3.3 CTC capture using the MOA microfluidic filter

Once we confirmed the feasibility of selective size amplification of CTCs with microbeads and the SOG fabrication of the MOA filter, we observed the movement of cells passing through the filter. High-speed photographic images clearly showed the WBCs, being relatively small, transiting the filter without any trapping and with minimal deformation (Fig. 3A). We observed MCF-7 breast cancer cells (without microbeads) to experience cell deformations even with cells larger than 20 μm in diameter (Fig. 3B). For a cell to pass the MOA filter gap, the time elapsed between the first (Fig. 3B1–B3) and second (Fig. 3B4–B5) gaps was similar, in concordance with simulations suggesting analogous fluidic forces in both filter gaps.

On the other hand, we observed that the cells size-amplified with microbeads *did not* experience deformation when stably captured within the MOA filter. Interestingly, in the case of cancer cells partially covered with microbeads, deformation was observed at the first filter gap with the portion of the cell surface denuded of microbeads directly contacting the filter gap (Fig. 3C1 and C2). Within the second filter gap, however, the microbeads covering the cancer cell were caught, resulting in stable CTC capture (Fig. 3C3 to Fig. 3C5). This qualitative result demonstrated that selective size amplification with solid microbeads and MOA microfiltration has unique benefits for CTC isolation by virtues of increased cell size and very importantly, reduced cell deformation (solid microbead effect).

Because we anticipated some heterogeneity in cell dimensions, we fabricated the microfluidic MOA filter chip with several filter gaps ranging between 8 μm and 30 μm. The size-amplified breast cancer cells were isolated in size-gradient filters in a non-normal distribution and this result showed that differently sized cancer cells were properly positioned, reducing compressive stresses. We also analyzed the proportion of cells captured between the first and second filter gaps. When these gaps were the same size, the percentage of cells captured within the 'cell capture room' was 43.5%. When the first filter gap was 2 μm larger than the second, the capture rate increased to 90.6%.

We also confirmed the relationship of the recovery rate as a function of different levels of selective size amplification by varying the microbead diameter. Based on the several references that characterized CTC isolation performance,[6,7,29] we decided on the CTC spiking number and 100 cancer cells with microbeads were 'spiked' with 1 mL of whole blood and this sample was injected into the microfluidic chip at a flow rate of 20 μL min^{-1}. Cell staining (DAPI, cytokeratin and CD45) after the filtration process clearly discriminated between WBCs (Fig. 4C) and CTCs (Fig. 4D); we were also able to determine cell numbers in order to compute recovery rate and purity. When a control sample of native (non-microbead associated) breast cancer cells were injected into the MOA filter chip, the recovery rate was less than 20%. By filtering cells bound with microbeads of varying sizes, recovery rates exceeding 85% were observed (Fig. 5). Though recovery rates with 5 μm microbeads were high, the filter was sometimes blocked by clusters of these microbeads and their low coverage over the CTC surface seemed to be the cause of this recovery rate variability. From this we confirmed that 3 μm

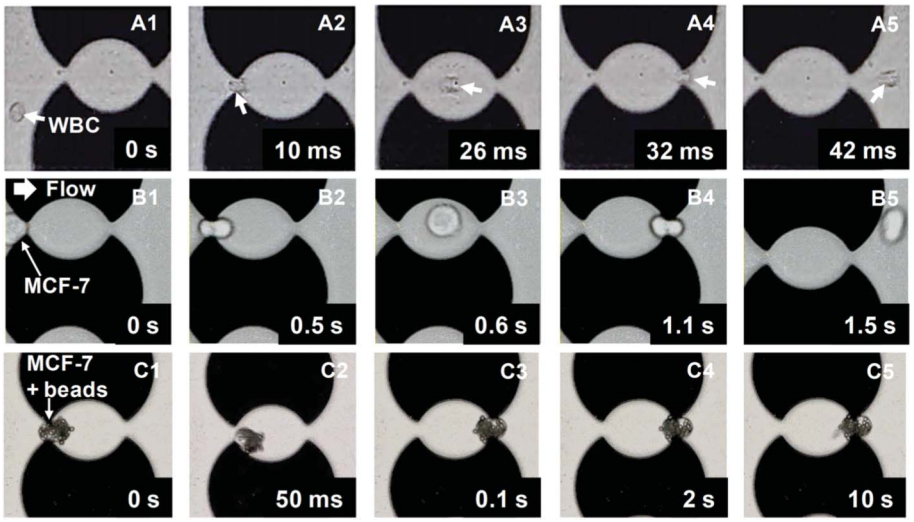

Fig. 3 High speed images depicting the movements of a WBC, an original MCF-7 cell and a size-amplified MCF-7 cell. (**A1–A5**) Images of a WBC passing through the MOA filter. (**B1–B5**) Images of an original MCF-7 cell passing through the MOA filter. (**C1–C5**) Images of a size-amplified MCF-7 cell passing through the MOA filter. The cancer cell covered with microbeads was stably captured showing that the SSA-MOA method offers unique benefits for cell isolation: increased cell size leading to an improved recovery rate and the solid microbead effect of mitigating cell deformation.

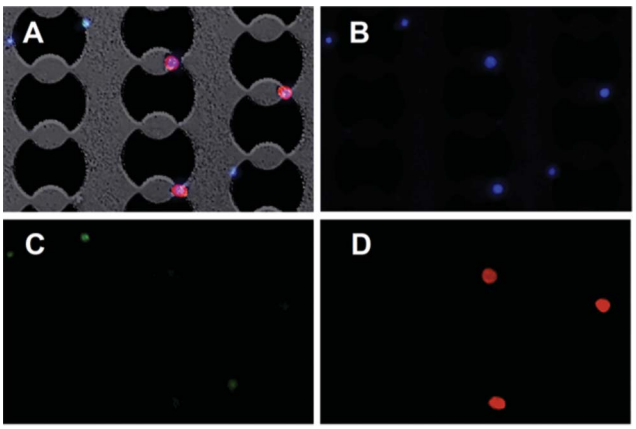

Fig. 4 Staining images after CTC isolation from whole blood. (**A**) A merged image stained for DAPI, CD45 and cytokeratin. (**B**) DAPI stain. (**C**) CD45 stain. (**D**) Cytokeratin stain. The red color and cell morphologies clearly identify the size-amplified cells.

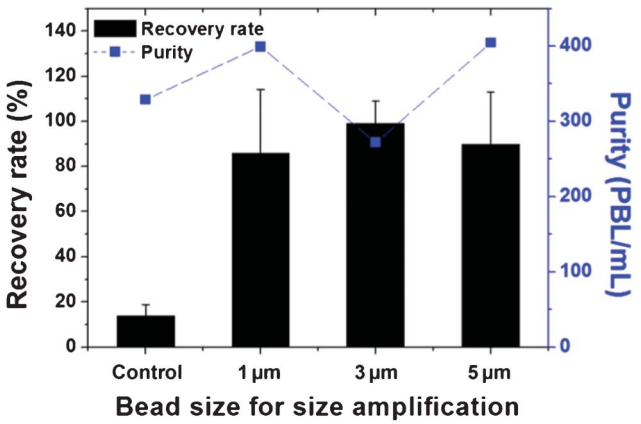

Fig. 5 Recovery rate and purity as a function of microbead size resulting in selective size amplification (n = 3). For MCF-7 cells isolated without microbeads (without selective size amplification), a recovery rate less than 20% was observed. In contrast, with size amplification, recovery rates exceeding 85% could be achieved for every size of microbeads with 3 μm microbeads having the highest recovery rate (99.1%). The concentration (per millilitre) of peripheral blood leukocytes (PBL) remained in the range of 272 to 405, with an average of 351 PBL mL^{-1}.

microbeads optimized the recovery rate (at 99.1%) and ensured stable capture without filter blockage. In addition, we tested the recovery rate under conditions of 10 cells per mL and results showed 89.7% recovery rate (n = 7) with cell size amplification of 3 μm microbeads.

After confirming the recovery rate, the MOA filter chip was evaluated for purity results. Peripheral blood leukocytes per millilitre remained from 272 to 405 in the MOA filter chip. As shown, however, in Fig. 4, the WBCs were non-specifically bound to the filter surfaces and those captured from the MOA filter were not observed. Therefore, the number of WBCs—the purity level—did not correlate with microbead size but rather was a function of the surface treatment of the filter and various blood characteristics. The method's purity demonstrated excellent performance as compared to other size-based separations (2000–10 000 PBL mL^{-1})[2,12,28] showing that this approach can, in principle, achieve high purities. From the result, the MOA platform showed the possibility of satisfying both high recovery rate and purity.

4. Conclusion

Many clinical studies have suggested a potential role for CTCs in cancer prognosis, therapeutic monitoring, and clinical decision-making. In order to realize such applications, CTC separation technologies must offer higher performance, in *both* recovery rate and purity. We introduce a novel CTC isolation method using selective size amplification (SSA) for target cells and a multi-obstacle architecture (MOA) microfluidic filter which offers advantages not only in resolving the trade-off between

recovery rate and purity—optimizing both—but also in reducing the mechanical stress exerted upon the CTCs during filter transit. The major reasons for this enhanced performance include distinctive size discrimination between WBCs and CTCs as well as the benefits of the solid microbeads mitigating cell deformation within the MOA filter gap. As a proof of concept, although the SSA-MOA method successfully isolated the MCF-7 cancer cells from whole blood samples, throughput improvements and a subsequent surface treatment step to remove non-specific binding is required. Moreover, as the method's specificity described in this paper is based on the EpCAM antibody, size amplification using alternative (or multiple) antibodies should also be considered. The SSA-MOA technology represents a potentially significant advance towards ensuring highly efficient isolation of these sparsely populated target cells in microfilter study contributing, therefore, to the sensitive and robust clinical validation of studies with CTCs and their applications.

Acknowledgements

We wish to acknowledge June-Young Lee, Sanghyun Baek, Jin-Mi Oh and Hun Joo Lee for their involvement in experimental work, as well as Jinhoon Kim and Wonho Lee for advice regarding simulation. We acknowledge again the contributions of the Yonsei University clinical study participants. This work was supported by the Bio Research Center at the Samsung Advanced Institute of Technology.

References

1 K. Pantel, R. H. Brakenhoff and B. Brandt, *Nat. Rev. Cancer*, 2008, **8**, 329–340.
2 P. Paterlini-Brechot and N. L. Benali, *Cancer Lett.*, 2007, **253**, 180–204.
3 D. Mavroudis, *Ann. Oncol.*, 2010, **21**(Supplement 7), vii95–100.
4 W. J. Allard, J. Matera, M. C. Miller, M. Repollet, M. C. Connelly, C. Rao, A. G. Tibbe, J. W. Uhr and L. W. Terstappen, *Clin. Cancer Res.*, 2004, **10**, 6897–6904.
5 L. Xi, D. G. Nicastri, T. El-Hefnawy, S. J. Hughes, J. D. Luketich and T. E. Godfrey, *Clin. Chem.*, 2007, **53**, 1206–1215.
6 S. Nagrath, L. V. Sequist, S. Maheswaran, D. W. Bell, D. Irimia, L. Ulkus, M. R. Smith, E. L. Kwak, S. Digumarthy, A. Muzikansky, P. Ryan, U. J. Balis, R. G. Tompkins, D. A. Haber and M. Toner, *Nature*, 2007, **450**, 1235–1239.
7 J. P. Gleghorn, E. D. Pratt, D. Denning, H. Liu, N. H. Bander, S. T. Tagawa, D. M. Nanus, P. A. Giannakakou and B. J. Kirby, *Lab Chip*, 2010, **10**, 27–29.
8 A. H. Talasaz, A. A. Powell, D. E. Huber, J. G. Berbee, K. H. Roh, W. Yu, W. Xiao, M. M. Davis, R. F. Pease, M. N. Mindrinos, S. S. Jeffrey and R. W. Davis, *Proc. Natl. Acad. Sci. U. S. A.*, 2009, **106**, 3970–3975.
9 M. Naoe, Y. Ogawa, J. Morita, K. Omori, K. Takeshita, T. Shichijyo, T. Okumura, A. Igarashi, A. Yanaihara, S. Iwamoto, T. Fukagai, A. Miyazaki and H. Yoshida, *Cancer*, 2007, **109**, 1439–1445.
10 R. Gertler, R. Rosenberg, K. Fuehrer, M. Dahm, H. Nekarda and J. R. Siewert, *Recent Results Cancer Res.*, 2003, **162**, 149–155.
11 T. M. Morgan, P. H. Lange and R. L. Vessella, *Front. Biosci.*, 2007, **12**, 3000–3009.
12 G. Vona, A. Sabile, M. Louha, V. Sitruk, S. Romana, K. Schutze, F. Capron, D. Franco, M. Pazzagli, M. Vekemans, B. Lacour, C. Brechot and P. Paterlini-Brechot, *Am. J. Pathol.*, 2000, **156**, 57–63.
13 S. Zheng, H. Lin, J. Q. Liu, M. Balic, R. Datar, R. J. Cote and Y. C. Tai, *J. Chromatogr., A*, 2007, **1162**, 154–161.
14 H. Mohamed, M. Murray, J. N. Turner and M. Caggana, *J. Chromatogr., A*, 2009, **1216**, 8289–8295.
15 S. J. Tan, L. Yobas, G. Y. Lee, C. N. Ong and C. T. Lim, *Biomed. Microdevices*, 2009, **11**, 883–892.
16 M. Hosokawa, T. Hayata, Y. Fukuda, A. Arakaki, T. Yoshino, T. Tanaka and T. Matsunaga, *Anal. Chem.*, 2010, **82**, 6629–6635.
17 P. R. Gascoyne, J. Noshari, T. J. Anderson and F. F. Becker, *Electrophoresis*, 2009, **30**, 1388–1398.
18 I. Cruz, J. Ciudad, J. J. Cruz, M. Ramos, A. Gomez-Alonso, J. C. Adansa, C. Rodriguez and A. Orfao, *Am. J. Clin. Pathol.*, 2005, **123**, 66–74.
19 D. Marrinucci, K. Bethel, R. H. Bruce, D. N. Curry, B. Hsieh, M. Humphrey, R. T. Krivacic, J. Kroener, L. Kroener, A. Ladanyi, N. H. Lazarus, J. Nieva and P. Kuhn, *Hum. Pathol.*, 2007, **38**, 514–519.
20 M. Yu, S. Stott, M. Toner, S. Maheswaran and D. A. Haber, *J. Cell Biol.*, 2011, **192**, 373–382.
21 S. Meng, D. Tripathy, E. P. Frenkel, S. Shete, E. Z. Naftalis, J. F. Huth, P. D. Beitsch, M. Leitch, S. Hoover, D. Euhus, B. Haley, L. Morrison, T. P. Fleming, D. Herlyn, L. W. Terstappen, T. Fehm, T. F. Tucker, N. Lane, J. Wang and J. W. Uhr, *Clin. Cancer Res.*, 2004, **10**, 8152–8162.
22 G. Deng, M. Herrler, D. Burgess, E. Manna, D. Krag and J. F. Burke, *Breast Cancer Res.*, 2008, **10**, R69.
23 M. Yang, C. W. Li and J. Yang, *Anal. Chem.*, 2002, **74**, 3991–4001.
24 J. S. de Bono, H. I. Scher, R. B. Montgomery, C. Parker, M. C. Miller, H. Tissing, G. V. Doyle, L. W. Terstappen, K. J. Pienta and D. Raghavan, *Clin. Cancer Res.*, 2008, **14**, 6302–6309.
25 M. Cristofanilli, G. T. Budd, M. J. Ellis, A. Stopeck, J. Matera, M. C. Miller, J. M. Reuben, G. V. Doyle, W. J. Allard, L. W. Terstappen and D. F. Hayes, *N. Engl. J. Med.*, 2004, **351**, 781–791.
26 M. Cristofanilli and J. Mendelsohn, *Proc. Natl. Acad. Sci. U. S. A.*, 2006, **103**, 17073–17074.
27 T. Fehm and W. Sauerbrei, *Breast Cancer Res. Treat.*, 2010, **122**, 219–220.
28 L. Zabaglo, M. G. Ormerod, M. Parton, A. Ring, I. E. Smith and M. Dowsett, *Cytometry*, 2003, **55A**, 102–108.
29 S. L. Stott, C. H. Hsu, D. I. Tsukrov, M. Yu, D. T. Miyamoto, B. A. Waltman, S. M. Rothenberg, A. M. Shah, M. E. Smas, G. K. Korir, F. P. Floyd Jr, A. J. Gilman, J. B. Lord, D. Winokur, S. Springer, D. Irimia, S. Nagrath, L. V. Sequist, R. J. Lee, K. J. Isselbacher, S. Maheswaran, D. A. Haber and M. Toner, *Proc. Natl. Acad. Sci. U. S. A.*, 2010, **107**, 18392–18397.

